Date of publication xxxx 00, 0000, date of current version xxxx 00, 0000.

Digital Object Identifier 10.1109/ACCESS.2017.DOI

Orthogonally Precoded Massive MIMO for High Mobility Scenarios

T. ZEMEN[1], (Senior Member, IEEE), D. LÖSCHENBRAND[1](Student Member, IEEE), M. HOFER[1](Student Member, IEEE), C. PACHER[1](Member, IEEE) and B. RAINER.[1], (Member, IEEE)

[1]AIT Austrian Insitute of Technology, Vienna

Corresponding author: T. Zemen (e-mail: thomas.zemen@ait.ac.at).

Thomas Zemen (thomas.zemen@ait.ac.at), David Löschenbrand, Markus Hofer, and Christoph Pacher are with AIT Austrian Institute of Technology, Vienna, Austria. This work is funded by the Austrian Research Promotion Agency (FFG) and the Austrian Ministry for Transport, Innovation and Technology (bmvit) within the project MARCONI (861208) of the funding program ICT of the Future. We would like to thank I. Glendinning for his support in improving the English language of this paper.

ABSTRACT Massive multiple-input multiple-output (MIMO) systems are of high interest for ultra-reliable low-latency communication (URLLC) links. They provide channel hardening, i.e. reduced channel variations, due to the large number of transmit antennas which exploit spatial diversity by beam-forming. Massive MIMO requires channel state information (CSI) on the base station side. For time-varying vehicular communication channels the CSI acquired during the uplink phase will be outdated for the following downlink phase, leading to reduced spatial channel hardening. We investigate a combination of massive MIMO with general orthogonal precoding (OP) to compensate this effect. OP uses two-dimensional precoding sequences in the time-frequency domain and provides channel hardening by exploiting time- and frequency diversity. We show that the combination of massive MIMO and OP is beneficial for time-varying communication channels. While the spatial channel hardening of massive MIMO decreases, the time-frequency channel hardening of OP increases with larger time-variance of the communication channel. An iterative receiver algorithm for massive MIMO with OP as well as a detailed analysis of the channel hardening effect is presented. We demonstrate a BER reduction by more than one order of magnitude for a velocity of $50\,\text{km/h} = 16,6\,\text{m/s}$ using the orthogonal frequency division multiplexing (OFDM) based 5G new radio (NR) physical layer.

INDEX TERMS 5G, massive MIMO, orthogonal precoding, ultra-reliable low-latency communication (URLLC) links

I. INTRODUCTION

Ultra-reliable low-latency wireless communication (URLLC) links are an important component for connected autonomous vehicles, industrial wireless control loops, and many other machine-to-machine communication applications [1]. The random fading process in wireless communication channels leads to signal strength fluctuations at the receive antenna and random unpredictable frame errors.

Massive multiple-input multiple-output (MIMO) systems reach the capacity of multi-user MIMO systems by linear beam-forming over a large number of transmit antenna elements on the base station side [2], achieving spatial channel hardening [3], [4]. Beam-forming requires channel state information (CSI) on the transmitter side, which is obtained during a preceding uplink phase by exploiting channel reciprocity in a time-division duplex (TDD) system.

Channel hardening reduces the random field-strength variation on the mobile station (MS) side. Hence, for URLLC links it is highly desirable to maximize channel hardening by appropriate pre-processing on the transmitter side.

For mobile users the channel impulse response is time-varying, hence the CSI becomes outdated (channel aging) due to the time delay between uplink and downlink transmission. This causes the channel hardening effect of massive MIMO to decrease with longer frame duration and increasing user velocity [5]. Previous work either considers a quasi static scenario where the uplink and downlink phase take part within a so called coherence interval [2] or performs channel prediction between the uplink and downlink transmission [5], [6] using long-term statistical information.

Another method to improve the communication link reliability is orthogonal precoding (OP) [7]–[10]. OP spreads a data symbol in the time-frequency domain and thus, achieves also channel hardening, i.e. the fading variation of the received signal strength can be strongly reduced [7]. The channel hardening effect of OP increases with increasing time- and frequency selectivity (larger delay and Doppler spread) of the communication channel.

CONTRIBUTIONS OF THE PAPER:

- In doubly selective channels, we propose to compensate for the lost spatial channel hardening of massive MIMO by improved time-frequency channel hardening due to OP [11].
- We present a receiver structure for massive MIMO with general OP that uses parallel interference cancellation (PIC) [12] and iterative channel estimation [13], applying a well-known low-complexity multi-user detection framework [14].
- We prove that any complete set of basis functions with constant modulus will achieve the same performance for massive MIMO with OP [7]. Furthermore, we analytically quantify the channel hardening effect of massive MIMO with OP for doubly-selective channels.
- We validate our theoretical results by numerical link level simulations for an infrastructure-to-vehicle URLLC communication link, using the 5G NR physical layer.

NOTATION:

We denote a scalar by a, a column vector by $\boldsymbol{a}$ and its i-th element with a_i. Similarly, we denote a matrix by $\boldsymbol{A}$ and its (i,ℓ)-th element by $a_{i,\ell}$. The transpose of $\boldsymbol{A}$ is given by $\boldsymbol{A}^{\mathrm{T}}$ and its conjugate transpose by $\boldsymbol{A}^{\mathrm{H}}$. A diagonal matrix with elements a_i is written as $\mathrm{diag}(\boldsymbol{a})$ and the $Q \times Q$ identity matrix as $\boldsymbol{I}_Q$, respectively. The absolute value of a is denoted by $|a|$ and its complex conjugate by a^*. The cardinality of set $\mathcal{I}$ is denoted by $|\mathcal{I}|$. We denote the set of all complex numbers by $\mathbb{C}$. The all one (zero) column vector with Q elements is denoted by $\mathbf{1}_Q$ ($\mathbf{0}_Q$). We identify the 2D sequence $(a_{i,\ell}) \in \mathbb{C}^{N\times M}$ for $i \in \{0,\ldots,N-1\}, \ell \in \{0,\ldots,M-1\}$ with the matrix $\boldsymbol{A} \in \mathbb{C}^{N\times M}$, i.e., $\boldsymbol{A} = (a_{i,\ell})$. Furthermore, we define the notation $\boldsymbol{a} = \mathrm{vec}(\boldsymbol{A}) = \mathrm{vec}\big((a_{i,\ell})\big) \in \mathbb{C}^{MN\times 1}$, where $\mathrm{vec}(\boldsymbol{A})$ denotes the vectorized version of matrix $\boldsymbol{A}$, formed by stacking the columns of $\boldsymbol{A}$ into a single column vector.

ORGANIZATION OF THE PAPER:

We present the signal model for massive MIMO with OP in Sec. II. An iterative symbol-wise ML detection algorithm and an iterative channel estimation algorithm are introduced in Sec. III and Sec. IV, respectively. We analyze the channel hardening effect of massive MIMO with OP in Sec. V. In Sec. VI numerical simulation results for OP are shown. We conclude in Sec. VII.

II. SIGNAL MODEL FOR MASSIVE MIMO WITH ORTHOGONAL PRECODING

In this work we are concerned with URLLC links for highly mobile users. Hence, the typical packet duration is short and the required reliability of the communication link shall be as high as possible. Due to short packet length the diversity utilized by the channel code is limited. Hence, additional linear precoding methods are crucial to exploit the full channel diversity in time, frequency and space, enabling URLLC.

We combine two linear preprocessing techniques in this work:

- The first one is OP, which exploits diversity in the time-frequency domain, and is applied once for each data packet. OP achieves channel hardening by precoding on the transmitter side and parallel interference cancellation (PIC) on the receiver side [7]. The channel hardening effect of OP increases with the delay- and Doppler spread of the doubly selective fading process, as well as with increasing extent of the precoding region in time- and frequency [7].
- The second preprocessing technique is maximum-ratio beam-forming in a massive MIMO system. Beamforming uses weights that are specific for each antenna element on the transmitter side. It achieves channel hardening that increases with the number of transmit antennas but decreases with (a) increasing frame duration and (b) increasing velocity of the mobile station, due to channel aging.

Throughout the paper, we will use the term precoding to describe linear operations performed in the time-frequency domain and the term beam-forming for the linear operations in the spatial domain.

A. PRECODING

We precode data symbols $b_{p,n} \in \mathcal{A}$, $p \in \{0,\ldots,N-1\}$, $n \in \{0,\ldots,M-1\}$, from the finite alphabet $\mathcal{A}$, on a transform domain grid (p,n) with a general complete set of 2D orthonormal basis functions:

$$d_{q,m} = \sum_{p=0}^{N-1}\sum_{n=0}^{M-1} b_{p,n} s_{q,m}^{p,n}, \tag{1}$$

where $s_{q,m}^{p,n}$ denotes two-dimensional precoding sequences and $d_{q,m}$ the result of the precoding operation, respectively. The time-frequency grid is defined by the discrete time index $m \in \{0,\ldots,M-1\}$ and the discrete frequency index $q \in \{0,\ldots,N-1\}$.

Let $\boldsymbol{B} \in \mathcal{A}^{N\times M}$ denote the symbol matrix with elements $b_{p,n}$. We define the symbol vector $\boldsymbol{b} = \mathrm{vec}(\boldsymbol{B}) = \mathrm{vec}\big((b_{p,n})\big) \in \mathcal{A}^{MN\times 1}$, and the precoded symbol vector $\boldsymbol{d} = \mathrm{vec}\big((d_{q,m})\big)$, using the notation introduced in Sec. I. Matrix

$$\boldsymbol{S} = [\boldsymbol{s}_{0,0},\ldots,\boldsymbol{s}_{N-1,0},\boldsymbol{s}_{0,1},\ldots,\boldsymbol{s}_{N-1,M-1}]^{\mathrm{T}} \in \mathbb{C}^{MN\times MN} \tag{2}$$

collects all vectorized 2D precoding sequences $\boldsymbol{s}_{p,n} = \mathrm{vec}\big((s^{p,n}_{q,m})\big) \in \mathbb{C}^{MN\times 1}$ column-wise. With these definitions, we can write (1) in vector matrix notation as

$$\boldsymbol{d} = \boldsymbol{S}\boldsymbol{b}\,. \tag{3}$$

In this work we will use a general OP formulation that is suitable for any set of orthogonal basis functions, enabling a direct comparison of different precoding methods. We will use three exemplary basis function sets for OP in this paper. Two sets contain constant modulus sequences, the basis functions of the discrete symplectic Fourier transform (DSFT) that are used for orthogonal time-frequency-space (OTFS) [8], [9] and the Walsh-Hadamard transform (WHT), respectively. One basis function set contains general orthonormal sequences, namely 2D discrete prolate spheroidal (DPS) sequences.

1) Discrete Symplectic Fourier Transform Sequences

The DSFT precoding sequences [8] are defined as

$$s^{p,n\ (\mathrm{DSFT})}_{q,m} = \frac{1}{\sqrt{MN}} \mathrm{e}^{\mathrm{j}2\pi(mn/M - qp/N)}\,. \tag{4}$$

2) Walsh-Hadamard Transform Sequences

We define the WHT precoding matrix recursively:

$$\boldsymbol{S}_2{}^{(\mathrm{WHT})} = \frac{1}{\sqrt{2}} \begin{bmatrix} 1 & 1 \\ 1 & -1 \end{bmatrix} \tag{5}$$

and

$$\boldsymbol{S}_{2r}{}^{(\mathrm{WHT})} = \frac{1}{\sqrt{2}} \begin{bmatrix} \boldsymbol{S}_r^{(\mathrm{WHT})} & \boldsymbol{S}_r^{(\mathrm{WHT})} \\ \boldsymbol{S}_r^{(\mathrm{WHT})} & -\boldsymbol{S}_r^{(\mathrm{WHT})} \end{bmatrix}. \tag{6}$$

The columns of $\boldsymbol{S}^{(\mathrm{WHT})}$ are denoted by $\boldsymbol{s}^{(\mathrm{WHT})}_{p,n}$.

3) 2D Discrete Prolate Spheroidal (2DDPS) Sequences

We define a general set of orthonormal basis functions as the product of two DPS sequences:

$$s^{p,n\ (\mathrm{2DDPS})}_{q,m} = u_{n,m}(W_\mathrm{t}, I_\mathrm{t}) u_{p,q}(W_\mathrm{f}, I_\mathrm{f}) \tag{7}$$

with $W_\mathrm{t} = [-\nu_\mathrm{D}, \nu_\mathrm{D}]$, $W_\mathrm{f} = [0, \theta_\mathrm{P}]$, $I_\mathrm{t} = \{0, \ldots, M-1\}$ and $I_\mathrm{f} = \{0, \ldots, N-1\}$. The normalized single-sided Doppler bandwidth is defined as $\nu_\mathrm{D} = f_\mathrm{D} T_\mathrm{S}$, where T_S denotes the OFDM symbol duration (sampling interval in time). The normalized delay is $\theta_\mathrm{P} = \tau_P \Delta f$, where Δf denotes the subcarrier bandwidth (sampling interval in frequency). DPS sequences $u_{i,\ell}(W, I)$ are the solution to the eigenvalue problem [15]

$$\sum_{\ell=0}^{M-1} C_{\ell-m}(W) u_{i,\ell}(W, I) = \lambda_i(W, I) u_{i,m}(W, I) \tag{8}$$

for $m \in I$ with

$$C_k(W) = \int_W \mathrm{e}^{\mathrm{j}2\pi k\nu} \mathrm{d}\,\nu = \frac{1}{\mathrm{j}2\pi k}(\mathrm{e}^{\mathrm{j}2\pi k\nu_2} - \mathrm{e}^{\mathrm{j}2\pi k\nu_1}) \tag{9}$$

and $W = [\nu_1, \nu_2]$. The eigenvalues $\lambda_i(W, I)$ are clustered near 1 for $i \leq \lceil |W||I| \rceil$ and rapidly drop to zero for $i > \lceil |W||I| \rceil$.

B. MASSIVE MIMO BEAM-FORMING

The precoded data symbol vector $\boldsymbol{d}$ is transmitted from all A antenna elements of the massive MIMO base station after linear beam-forming. The samples received at the single antenna of the mobile station are

$$\boldsymbol{y} = \boldsymbol{G}^\mathrm{T} \boldsymbol{\Omega} \mathrm{diag}(\boldsymbol{\chi}) \boldsymbol{d} + \boldsymbol{n}\,, \tag{10}$$

where the massive MIMO channel matrix

$$\boldsymbol{G} = \begin{bmatrix} \mathrm{diag}(\boldsymbol{g}_1) \\ \vdots \\ \mathrm{diag}(\boldsymbol{g}_A) \end{bmatrix} \in \mathbb{C}^{MNA\times MN}\,. \tag{11}$$

The time-varying frequency response from antenna a to the mobile station is denoted by $\boldsymbol{g}_a = \mathrm{vec}\big((g^a_{q,m})\big) \in \mathbb{C}^{MN\times 1}$, $a \in \{1, \ldots, A\}$. The time-varying impulse response $h^a_{q,m}$ is defined as its Fourier transform. We use the normalization

$$\mathbb{E}\{||\boldsymbol{G}||_2^2\} = MN \tag{12}$$

such that the array gain is not taken into account and the channel gain is unity on average. Additive white complex symmetric Gaussian noise is denoted by $\boldsymbol{n}$ with zero mean and variance $\sigma_n^2 \boldsymbol{I}_{MN}$, $\boldsymbol{n} = \mathcal{CN}(0, \sigma_n^2 \boldsymbol{I}_{MN})$, the signal to noise ratio (SNR) on the receiver side is denoted by $1/\sigma_n^2$. Linear massive MIMO beam-forming is performed by

$$\boldsymbol{\Omega} = \begin{bmatrix} \mathrm{diag}(\boldsymbol{\omega}_1) \\ \vdots \\ \mathrm{diag}(\boldsymbol{\omega}_A) \end{bmatrix} \in \mathbb{C}^{MNA\times MN}\,, \tag{13}$$

where the beamforming weights for antenna a are denoted by $\boldsymbol{\omega}_a$ with elements $\omega^a_{q,m}$. The windowing function on the transmitter side is denoted by $\boldsymbol{\chi}$. We use a rectangular window $\boldsymbol{\chi} = \boldsymbol{1}_{MN}$ and drop $\boldsymbol{\chi}$ to simplify the notation in the remainder of the paper.

Vector $\boldsymbol{g}_a$ represents the combined result of OFDM modulation, the doubly selective channel, and OFDM demodulation between base station antenna a and the mobile station. We assume a proper OFDM system design where the doubly selective channel does not cause inter-symbol interference (ISI), and the inter-carrier interference (ICI) is small enough to be neglected. These are realistic assumptions for vehicular communication systems using 5G NR with an appropriate parameterization. See the detailed discussion in [16, Sec. II]. The numerical results shown in Section VI use a geometry-based channel model and potential ICI or ISI effects will be taken into account.

The combined channel between transmitter and receiver including massive MIMO beam-forming weights results in a diagonal matrix

$$\mathrm{diag}(\boldsymbol{\phi}) = \boldsymbol{G}^\mathrm{T} \boldsymbol{\Omega} \in \mathbb{C}^{MN\times MN} \tag{14}$$

with

$$\boldsymbol{\phi} = \mathrm{vec}\big((\phi_{q,m})\big) = \mathrm{vec}\Big(\big(\sum_{a=1}^{A} g^a_{q,m}\, \omega^a_{q,m}\big)\Big)\,. \tag{15}$$

Inserting (14) into (10) we obtain

$$\boldsymbol{y} = \mathrm{diag}(\boldsymbol{\phi})\boldsymbol{S}\boldsymbol{b} + \boldsymbol{n}\,. \tag{16}$$

The effective spreading sequence is defined as $\tilde{\boldsymbol{S}} = \mathrm{diag}(\boldsymbol{\phi})\boldsymbol{S}$, resulting in

$$\boldsymbol{y} = \tilde{\boldsymbol{S}}\boldsymbol{b} + \boldsymbol{n}\,. \tag{17}$$

III. ITERATIVE DETECTION

The signal model for massive MIMO with OP in (17) is identical to the one used for multi-user detection in [12, (10)]. Multi-access interference in [12] is replaced by inter-symbol interference in this paper. Hence, we can employ the iterative PIC algorithm [7], [12], [14], [17] for symbol-wise maximum likelihood (ML) detection, using soft-symbol feedback.

The a-posteriori probability (APP) output of the soft-input soft-output BCJR decoder [18] is interleaved and mapped to the alphabet $\mathcal{A}$ to obtain soft symbols $\tilde{b}_{p,n}$ [12]. The system model for the transmitter, the convolution with a doubly selective massive MIMO channel, and the receiver is shown in Fig. 1.

We perform soft inter-symbol interference cancelation at iteration i for the symbol transmitted on grid point (p,n)

$$\tilde{\boldsymbol{y}}_{p,n}^{(i)} = \left(\boldsymbol{y} - \tilde{\boldsymbol{S}}\tilde{\boldsymbol{b}}^{(i-1)} + \tilde{\boldsymbol{s}}_{p,n}\tilde{b}_{p,n}^{(i-1)}\right)\,, \tag{18}$$

where the soft-symbol feedback vector $\tilde{\boldsymbol{b}}^{(i)} = \mathrm{vec}\big((\tilde{b}_{p,n}^{(i)})\big) \in \mathbb{C}^{MN\times 1}$.

The output of the interference canceler $\tilde{\boldsymbol{y}}_{p,n}^{(i)}$ is further cleaned from noise and inter-symbol interference with a successive linear minimum mean square error (MMSE) filter in order to obtain a code symbol estimate,

$$\alpha_{p,n}^{(i)} = \left(\boldsymbol{f}_{p,n}^{(i)}\right)^{\mathrm{H}} \tilde{\boldsymbol{y}}_{p,n}^{(i)}\,. \tag{19}$$

An unbiased conditional linear MMSE filter can be found similarly to the linear MMSE detector given in [12], [17]. To simplify the notation we omit the iteration index i for the filter. It has the form

$$\boldsymbol{f}_{p,n}^{\mathrm{H}} = \frac{\tilde{\boldsymbol{s}}_{p,n}^{\mathrm{H}}\left(\sigma_n^2\boldsymbol{I}_N + \tilde{\boldsymbol{S}}\boldsymbol{V}\tilde{\boldsymbol{S}}^{\mathrm{H}}\right)^{-1}}{\tilde{\boldsymbol{s}}_{p,n}^{\mathrm{H}}\left(\sigma_n^2\boldsymbol{I}_N + \tilde{\boldsymbol{S}}\boldsymbol{V}\tilde{\boldsymbol{S}}^{\mathrm{H}}\right)^{-1}\tilde{\boldsymbol{s}}_{p,n}}\,. \tag{20}$$

Matrix $\boldsymbol{V}$ denotes the error covariance matrix

$$\boldsymbol{V} = \mathbb{E}_{b}\left\{(\boldsymbol{b}-\tilde{\boldsymbol{b}})(\boldsymbol{b}-\tilde{\boldsymbol{b}})^{\mathrm{H}}\right\} \tag{21}$$

with diagonal elements

$$[\boldsymbol{V}]_{p+nM,p+nM} = 1 - |\tilde{b}_{p,n}^{(i)}|^2 \tag{22}$$

We use a low complexity approximation for the matrix inversion in (20) according to [19], resulting in

$$\boldsymbol{f}_{p,n}^{\mathrm{H}} \approx \frac{\tilde{\boldsymbol{s}}_{p,n}^{\mathrm{H}}\left(\sigma_n^2\boldsymbol{I}_N + \mathrm{diag}(\boldsymbol{\kappa})\right)^{-1}}{\tilde{\boldsymbol{s}}_{p,n}^{\mathrm{H}}\left(\sigma_n^2\boldsymbol{I}_N + \mathrm{diag}(\boldsymbol{\kappa})^{\mathrm{H}}\right)^{-1}\tilde{\boldsymbol{s}}_{p,n}}\,. \tag{23}$$

where the elements of $\boldsymbol{\kappa}$ are given as

$$\kappa_{q,m} = \hat{\sigma}_{\tilde{b}}^2\phi_{q,m}\,. \tag{24}$$

The sample variance of the soft-symbol feedback is estimated according to $\hat{\sigma}_{\tilde{b}}^2 = \frac{1}{NM}\sum_{p=0}^{N}\sum_{n=0}^{M}|\tilde{b}_{p,n}|^2$. Hence, in (23) a diagonal matrix needs to be inverted, i.e. only scalar divisions are needed.

Assuming perfect PIC and unbiased MMSE detection, i.e. $\boldsymbol{V} = \boldsymbol{0}$, we obtain

$$\alpha_{p,n}^{(i)} \approx \frac{\overbrace{\tilde{\boldsymbol{s}}_{p,n}^{\mathrm{H}}\tilde{\boldsymbol{s}}_{p,n}}^{\gamma_{p,n}}\,b_{p,n} + \tilde{\boldsymbol{s}}_{p,n}^{\mathrm{H}}\boldsymbol{n}}{\tilde{\boldsymbol{s}}_{p,n}^{\mathrm{H}}\tilde{\boldsymbol{s}}_{p,n}} \tag{25a}$$

$$= b_{p,n} + \frac{1}{\gamma_{p,n}}\tilde{n}_{p,n}\,, \tag{25b}$$

where the effective channel coefficient is denoted by $\gamma_{p,n}$. Noise $\tilde{n}_{p,n}$ has the same distribution as $n_{q,m}$. The resulting noise variance for the detection of $b_{p,n}$ is scaled by the effective channel $\gamma_{p,n}$.

The symbol-wise ML expression

$$\hat{b}_{p,n} = \underset{b_{p,n}\in\mathcal{A}}{\mathrm{argmin}}\{|\alpha_{p,n} - b_{p,n}|^2\} \tag{26}$$

for data symbol $b_{p,n}$ is formulated based on the scalar signal model (25b). A soft-output sphere decoder [20], using (26), supplies log-likelihood ratios (LLRs) L_k. The LLRs are used as input for the BCJR decoder [18].

IV. ITERATIVE CHANNEL ESTIMATION

Channel estimation can be strongly simplified for massive MIMO systems in slowly time-varying channels due to channel hardening [4]. However, this requires perfect CSI on the base station side which is difficult to maintain in highly time-varying vehicular scenarios.

For vehicular communication links we need to obtain estimates of the combined channel $\boldsymbol{\phi}$ for coherent detection at the mobile station. Hence, we interleave S_{p} pilot symbols $\boldsymbol{p} \in \mathbb{C}^{S_{\mathrm{p}}\times 1}$ with S_{d} precoded data symbols $\boldsymbol{d} \in \mathbb{C}^{S_{\mathrm{d}}\times 1}$ in the time-frequency domain, such that $S_{\mathrm{d}} + S_{\mathrm{p}} = MN$. We modify the signal model (16) and express the interleaving with a permutation matrix $\boldsymbol{P}$:

$$\boldsymbol{y} = \mathrm{diag}(\boldsymbol{\phi})\underbrace{[\boldsymbol{P}_{\mathrm{p}}\boldsymbol{P}_{\mathrm{d}}]}_{\boldsymbol{P}}\begin{bmatrix}\boldsymbol{p}\\ \boldsymbol{S}\boldsymbol{b}\end{bmatrix} + \boldsymbol{n}\,, \tag{27}$$

where $\boldsymbol{P}_{\mathrm{p}} \in \mathbb{R}^{MN\times S_{\mathrm{p}}}$ describes the pilot symbol placement and $\boldsymbol{P}_{\mathrm{d}} \in \mathbb{R}^{MN\times S_{\mathrm{d}}}$ the (precoded) data symbol positions in the time-frequency grid. All the equations in the previous Sections II and III are still valid by replacing M with M', N with N', and $\boldsymbol{g}$ with $\boldsymbol{P}_{\mathrm{d}}\boldsymbol{g}$, where $M' \le M$, $N' \le N$, and $S_{\mathrm{d}} = M'N'$.

For channel estimation, we rewrite (27) as

$$\boldsymbol{y} = \mathrm{diag}\left(\boldsymbol{P}_{\mathrm{p}}\boldsymbol{p} + \boldsymbol{P}_{\mathrm{d}}\boldsymbol{S}\boldsymbol{b}\right)\boldsymbol{\phi} + \boldsymbol{n}\,. \tag{28}$$

Following the derivation in [12, (30)-(39)], we obtain the Wiener filter for $\boldsymbol{\phi}$ as

$$\hat{\boldsymbol{\phi}} = \boldsymbol{R}_g\tilde{\boldsymbol{D}}^{\mathrm{H}}\left(\tilde{\boldsymbol{D}}\boldsymbol{R}_g\tilde{\boldsymbol{D}}^{\mathrm{H}} + \boldsymbol{\Lambda} + \sigma_z^2\boldsymbol{I}_{MN}\right)^{-1}\boldsymbol{y}\,. \tag{29}$$

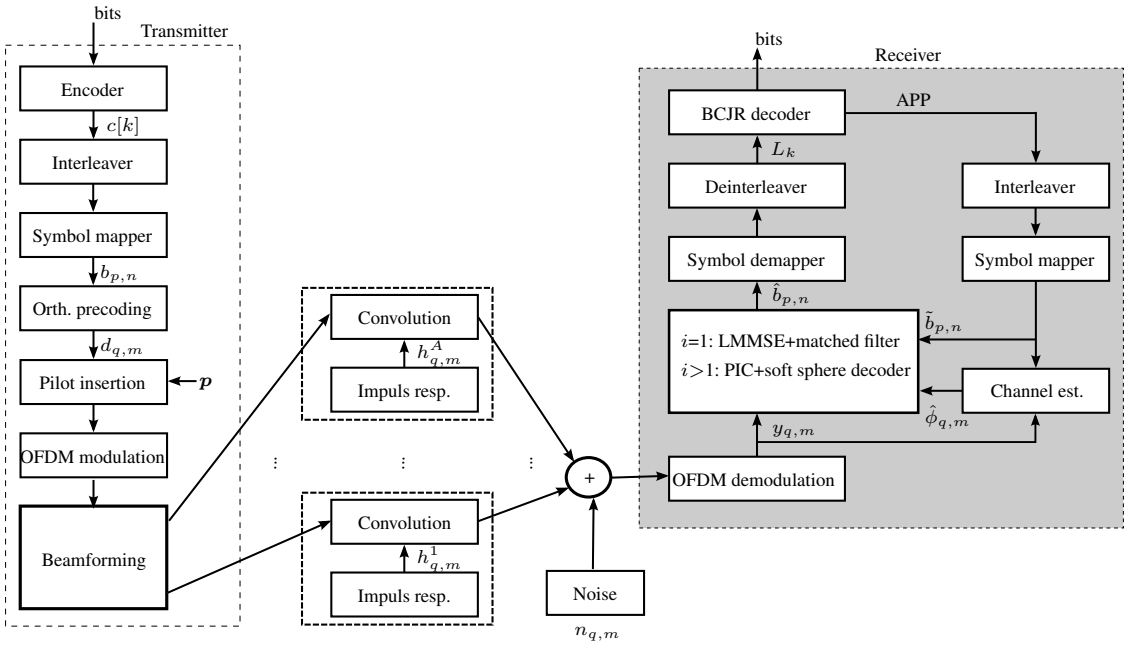

FIGURE 1. System model of the transmitter and iterative receiver for massive MIMO with OP.

The orthogonal precoded soft-symbol feedback is expressed as

$$\tilde{\boldsymbol{D}} = \mathrm{diag}\big(\boldsymbol{P}_{\mathrm{p}}\boldsymbol{p} + \boldsymbol{P}_{\mathrm{d}}\boldsymbol{S}\tilde{\boldsymbol{b}}\big)\,, \tag{30}$$

and

$$\boldsymbol{\Lambda} = \mathrm{diag}(\boldsymbol{P}_{\mathrm{p}}\boldsymbol{0}_{S_{\mathrm{p}}} + \boldsymbol{P}_{\mathrm{d}}\boldsymbol{1}_{S_{\mathrm{d}}}(1-\sigma^2_{\tilde{b}}))\,. \tag{31}$$

For time-frequency grid positions (q, m) where pilot symbols are transmitted, the corresponding entries on the diagonal of $\boldsymbol{\Lambda}$ are equal to zero. All other entries, related to precoded data-symbols, are filled with the variance of the soft-symbol feedback of the BCJR decoder.

The soft-symbol feedback is modeled as complex Gaussian distributed $\tilde{\boldsymbol{b}} \sim \mathcal{CN}(0, \sigma^2_{\tilde{b}}\boldsymbol{I}_{S_{\mathrm{d}}})$, with zero mean and variance $\sigma^2_{\tilde{b}}\boldsymbol{I}_{S_{\mathrm{d}}}$. Hence, if the output of the BCJR decoder converges towards the true transmit symbols, the term $(1-\sigma^2_{\tilde{b}})$ tends to zero, and (29) becomes a classic Wiener filter. The sample variance of the soft-symbol feedback is estimated according to $\hat{\sigma}^2_{\tilde{b}} = \frac{1}{S_{\mathrm{d}}}\sum_{p=0}^{N'-1}\sum_{n=0}^{M'-1}|\tilde{b}_{p,n}|^2$. The eigenvalue structure of the channel covariance matrix $\boldsymbol{R}_g = \mathbb{E}\{\boldsymbol{g}_a\boldsymbol{g}_a^{\mathrm{H}}\}$ can be exploited to implement a reduced rank version of (29), reducing the numerical complexity (see [13, (32)]).

V. CHANNEL HARDENING IN A MASSIVE MIMO SYSTEM WITH OP

In [21], massive MIMO beam-forming methods are compared, assuming accurate CSI is available on the base-station side. In URLLC applications for highly mobile users this assumption is hard to maintain. Hence, for time-varying scenarios, we investigate the joint usage of a massive MIMO system with OP aiming to minimize the bit error rate (BER).

For the joint analysis of a combined massive MIMO and OP system we focus on the scalar signal model for each data symbol in the transform domain (p, n) described by (25b). The probability density function (pdf) $f_\gamma(\gamma)$ of the effective channel coefficient

$$\gamma_{p,n}[f] = \tilde{\boldsymbol{s}}^{\mathrm{H}}_{p,n}\tilde{\boldsymbol{s}}_{p,n} = \tag{32a}$$

$$= \sum_{q=0}^{N-1}\sum_{m=(f-1)M}^{fM-1} s^{p,n\,*}_{q,m}\phi^*_{q,m}\phi_{q,m}s^{p,n}_{q,m} = \tag{32b}$$

$$= \sum_{q=0}^{N-1}\sum_{m=(f-1)M}^{fM-1} |s^{p,n}_{q,m}|^2|\phi_{q,m}|^2 = \tag{32c}$$

$$= \sum_{q=0}^{N-1}\sum_{m=(f-1)M}^{fM-1} |s^{p,n}_{q,m}|^2\left|\sum_{a=1}^{A} g^a_{q,m}\,\omega^a_{q,m}\right|^2 \tag{32d}$$

determines the performance of the communication system. The frame index $f \in \{1, \ldots, F\}$. Clearly, the distribution $f_\gamma(\gamma)$ shall have a large mean μ_γ and a small standard deviation σ_γ (root of the second central moment). This maximizes the channel hardening effect and minimizes the channel hardening measure β. It is defined as the ratio

$$\beta = \frac{\sigma_\gamma}{\mu_\gamma}\,, \tag{33}$$

following the definition in [3], [4]. The value of $\beta \to 0$ for $A, M, N \to \infty$.

From (32d) it becomes clear that $f_\gamma(\gamma)$ is determined by four factors:

A. The precoding sequences $s^{p,n}_{q,m}$,
B. the fading process $g^a_{q,m}$,

C. the beam-forming method at the base station represented by $\omega^a_{q,m}$, and
D. the error of the CSI used for beam-forming at the base station.

We will explore these four aspects in the following four sections.

A. PRECODING SEQUENCES

We treat two special cases:

a) No precoding (NO): In this case we can set $\boldsymbol{S} = \boldsymbol{I}$, i.e.

$$s^{p,n}_{q,m} = \begin{cases} 1 & \text{for} \quad p = q \quad \text{and} \quad n = m\,; \\ 0 & \text{otherwise,} \end{cases} \tag{34}$$

and obtain

$$\gamma^{\mathrm{NO}}_{p,n} = \left| \sum_{a=1}^{A} g^a_{q,m}\, \omega^a_{q,m} \right|^2 \tag{35}$$

with $p = q$ and $n = m$.

b) Precoding with constant modulus (CM) sequences: This case applies, e.g., for DSFT or WHT sequences, where

$$|s^{p,n}_{q,m}|^2 = \frac{1}{MN} \tag{36}$$

holds. We obtain

$$\gamma^{\mathrm{CM}}_{p,n} = \gamma^{\mathrm{CM}} = \frac{1}{MN} \sum_{q=0}^{N-1} \sum_{m=0}^{M-1} \left| \sum_{a=1}^{A} g^a_{q,m}\, \omega^a_{q,m} \right|^2 . \tag{37}$$

Please note that all grid elements (p, n) will be affected by the same effective channel condition γ^{CM}, hence we omit the grid index (p, n) in the following.

Equation (37) provides an important insight: All orthogonal constant modulus sequences will provide the same performance for OP. This means that doubly-selective channels do not require the usage of the DSFT. Hence, a transform between the time-frequency and the delay-Doppler domain is not required for the precoding of data symbols in doubly selective channels.

The conclusion above does not apply for channel estimation. The transform to the delay-Doppler domain by the DSFT might be beneficial for channel estimation, if precoded pilot-symbols are to be used and the doubly selective channel exhibits a sparse delay-Doppler representation [22], [23]

B. FADING PROCESS

We can express $\boldsymbol{g}_a$ as a filtered white Gaussian random process ,

$$\boldsymbol{g}_a = \boldsymbol{U} \sqrt{\boldsymbol{\Sigma}} \boldsymbol{U}^{\mathrm{H}} \boldsymbol{z}\,, \tag{38}$$

where $\boldsymbol{z} \sim \mathcal{CN}(0, \boldsymbol{I}_{MN})$ is a complex Gaussian random vector with independent identically distributed (i.i.d.) entries. Matrix $\boldsymbol{U}$ contains eigenvectors of the covariance matrix $\boldsymbol{R}_g$, and $\boldsymbol{\Sigma}$ contains eigenvalues λ_i on the main diagonal:

$$\boldsymbol{R}_g = \boldsymbol{U} \boldsymbol{\Sigma} \boldsymbol{U}^{\mathrm{H}}\,. \tag{39}$$

To simplify the analysis we assume the same time- and frequency correlation for all antenna elements a and independent channel realizations for each antenna element.

The direct evaluation of (39) for a general doubly-selective correlated fading processes is numerically difficult, due to the multiplicity of the largest eigenvalues of $\boldsymbol{R}_g$. A numerically stable algorithm for the calculation of λ_i for a fading process with a flat delay-Doppler scattering function is shown in [13]. This fading process is defined by two parameters, the normalized delay support θ_{P} and the normalized single-sided Doppler support ν_{D}. The correlation matrix is denoted by $\tilde{\boldsymbol{R}}_g(\nu_{\mathrm{D}}, \theta_{\mathrm{P}}; M, N)$, see [13, (26)-(28)]. Using the algorithm from [13] we can calculate the eigenvalues $\tilde{\lambda}_i(\nu_{\mathrm{D}}, \theta_{\mathrm{P}}; M, N)$ of $\tilde{\boldsymbol{R}}_g(\nu_{\mathrm{D}}, \theta_{\mathrm{P}}; M, N)$ numerically.

C. BEAM-FORMING METHOD

Without loss of generality, we focus on maximum ratio transmission with beamforming matrix [2], [21]

$$\boldsymbol{\Omega} = \frac{\tilde{\boldsymbol{G}}^*}{||\tilde{\boldsymbol{G}}||_2}\,, \tag{40}$$

i.e.

$$\omega^a_{q,m} = \frac{1}{||\tilde{\boldsymbol{G}}||_2}\, \tilde{g}^a_{q,m}{}^*\,, \tag{41}$$

where $\tilde{g}^a_{q,m}$ denotes the channel estimates on the base station side. The combined channel can be written as

$$\phi_{q,m} = \frac{1}{||\tilde{\boldsymbol{G}}||_2} \sum_{a=1}^{A} g^a_{q,m}\, \tilde{g}^a_{q,m}{}^*\,. \tag{42}$$

In the case of perfect CSI (PER CSI) the combined channel simplifies to

$$\phi_{q,m} = \frac{1}{||\boldsymbol{G}||_2} \sum_{a=1}^{A} |g^a_{q,m}|^2\,. \tag{43}$$

Hence, maximum-ratio combining is achieved for each element (q, m) of the time-frequency grid. With maximum-ratio beam-forming according to (40), the combined channel becomes almost frequency flat and non time-selective (assuming favorable propagation conditions). For $A \to \infty$ this conclusion becomes exact [2].

D. CSI USED FOR BEAM-FORMING

For the CSI at the base station we explore the following cases:

a) Perfect CSI: We assume the base station knows the time-varying CSI for the downlink perfectly, i.e., $\tilde{g}^a_{q,m} = g^a_{q,m}$.
b) Block fading (BF) CSI: The base station uses the last-known CSI, from the end of the uplink transmission, for precoding during the full downlink frame. Hence, $\tilde{g}^a_{q,m} = g^a_{q,-1} \quad \forall \quad m \in \{0, \ldots, M-1\}$.

In Fig. 2 we plot the absolute value of the combined channel $|\phi_{q,m}|$, versus time m and frequency q. With PER CSI a nearly frequency-flat and non time-selective frequency response is obtained. In the second example BF CSI is

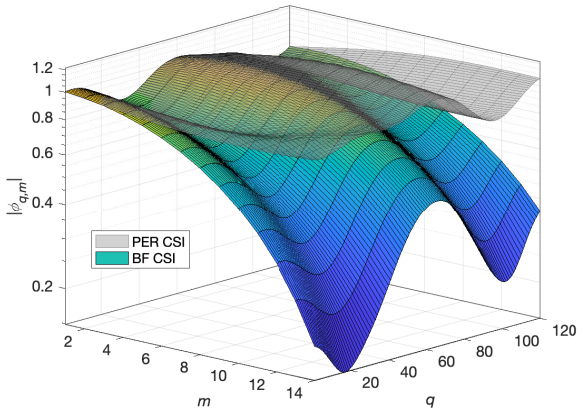

FIGURE 2. Absolute value of the combined channel $|\phi_{q,m}|$ for time-varying massive MIMO beam-forming with perfect (PER) CSI and for block-fading (BF) CSI. In both cases $A = 64$ antennas are used. The 5G NR physical layer parameters are defined in Table 1.

used. The channel aging effect is demonstrated, i.e., channel hardening decreases with increasing time m. The mean decreases and the standard deviation increases. The simulation parameters of the 5G NR physical layer are defined in Table 1.

E. EMPIRICAL EVALUATION OF CHANNEL HARDENING

For the pdf of γ in (32d) a closed from description is unknown for the general case. Hence, we need to resort to a numerical evaluation of the channel hardening effect for massive MIMO with OP. For the pdf $f_\gamma(\gamma)$ we can obtain the first moment

$$\mu_\gamma = \mathbb{E}\{\gamma\} = \frac{1}{NMF} \sum_{p=0}^{N-1} \sum_{n=0}^{M-1} \sum_{f=1}^{F} \gamma_{p,n}[f]\,, \tag{44}$$

and the square root of the second central moment

$$\sigma_\gamma = \sqrt{\mathbb{E}\{(\gamma - \mu_\gamma)^2\}} = \tag{45}$$

$$= \sqrt{\frac{1}{NMF-1} \sum_{p=0}^{N-1} \sum_{n=0}^{M-1} \sum_{f=1}^{F} (\gamma_{p,n}[f] - \mu_\gamma)^2}\,. \tag{46}$$

empirically by using F frame transmissions [3], [4].

F. ANALYTICAL CHANNEL HARDENING RESULTS FOR SPECIAL CASES

For a set of special cases an analytic treatment of the moments of $f_\gamma(\gamma)$ is indeed possible and we will explore this cases below.

1) Constant Modulus OP with a single transmit antenna

For the special case of constant modulus OP using a single transmit antenna $A = 1$ and without beamforming $\omega^a_{q,m} = 1$, we can show the channel hardening effect of OP analytically using the eigenvalue spectrum of $\boldsymbol{R}_g$. Inserting (38) in (37) we obtain

$$\gamma^{\mathrm{CM}} = \frac{1}{MN} \sum_{q=0}^{N-1} \sum_{m=0}^{M-1} \left|g^a_{q,m}\right|^2 = \frac{1}{MN} \boldsymbol{g}^{\mathrm{H}} \boldsymbol{g} = \tag{47a}$$

$$= \frac{1}{MN} \boldsymbol{z}^{\mathrm{H}} \boldsymbol{U} \sqrt{\boldsymbol{\Sigma}} \boldsymbol{U}^{\mathrm{H}} \boldsymbol{U} \sqrt{\boldsymbol{\Sigma}} \boldsymbol{U}^{\mathrm{H}} \boldsymbol{z} = \tag{47b}$$

$$= \frac{1}{MN} \sum_{i=0}^{MN-1} \lambda_i |\tilde{z}_i|^2\,, \tag{47c}$$

where $\tilde{\boldsymbol{z}} \sim \mathcal{CN}(0, \boldsymbol{I}_{MN})$, since $\boldsymbol{U}$ is a unitary matrix. It follows, that γ^{CM} is distributed according to a sum of independent exponentially distributed random variables weighted by eigenvalues λ_i. Its mean is

$$\mu_\gamma = \mathbb{E}\{\gamma\} = \frac{1}{MN} \sum_{i=0}^{MN-1} \lambda_i = 1\,, \tag{48}$$

since $\sum_{i=0}^{MN-1} \lambda_i = MN$. Its standard deviation is

$$\sigma_\gamma = \sqrt{\mathbb{E}\{(\gamma - \mu_\gamma)^2\}} = \frac{1}{MN} \sqrt{\sum_{i=0}^{MN-1} \lambda_i^2}\,. \tag{49}$$

Inserting the eigenvalues $\tilde{\lambda}_i(\nu_{\mathrm{D}}, \theta_{\mathrm{P}}; M, N)$ of $\tilde{\boldsymbol{R}}_g(\nu_{\mathrm{D}}, \theta_{\mathrm{P}}; M, N)$ in (49) we can obtain

$$\beta = \sigma_\gamma(\nu_{\mathrm{D}}, \theta_{\mathrm{P}}; M, N)/\mu_\gamma \tag{50}$$

for a fading process with flat power delay profile and flat Doppler spectral density. This result serves as lower bound for other fading processes with the same support.

2) Massive MIMO using PER CSI with constant modulus OP

For the case of PER CSI at the base station, a large number of antennas A and CM OP we can also obtain a closed form expression for the channel hardening measure β. We assume independence of antenna elements and M and N to be large [2], [4]. In this case spatial channel hardening and time-frequency channel hardening are multiplicative effects resulting in

$$\beta \approx \frac{1}{MN\sqrt{A}} \sqrt{\sum_{i=0}^{MN-1} \tilde{\lambda}_i(\nu_{\mathrm{D}}, \theta_{\mathrm{P}}; M, N)^2}\,. \tag{51}$$

We can obtain a simpler upper bound using the special shape of the eigenvalue spectrum described in Sec. II-A3 [24]. The essential subspace dimension in time is $D_t = \lceil 2\nu_{\mathrm{D}} M \rceil$ and in frequency it is $D_f = \lceil \theta_{\mathrm{P}} N \rceil$. Just modeling the largest eigenvalues of $\tilde{\boldsymbol{R}}_g(\nu_{\mathrm{D}}, \theta_{\mathrm{P}}; M, N)$, for large M and N we obtain the following upper bound:

$$\beta < \overline{\beta} = \frac{1}{MN\sqrt{A}} \frac{1}{2\nu_{\mathrm{D}}\theta_{\mathrm{P}}} \sqrt{(\lceil 2\nu_{\mathrm{D}} M \rceil)\,(\lceil \theta_{\mathrm{P}} N \rceil)}\,. \tag{52}$$

See also [13, (26)-(28)]. Relaxing the ceiling operator we obtain the intuitive expression

$$\beta < \overline{\beta} = \sqrt{\frac{1}{2\nu_{\mathrm{D}}\theta_{\mathrm{P}} MNA}}, \tag{53}$$

for an upper bound of the channel hardening measure β.

TABLE 1. Simulation Parameters for 5G NR

Name	Variable	Value
FFT size	N_{FFT}	512
used subcarriers	N	120
OFDM symbols	M	12
subcarrier bandwidth	Δf	15 kHz
bandwidth	B	7.68 MHz
cyclic prefix	G	40
carrier frequency	f_{C}	5.9 GHz
antennas at BS	A	64
pilot OFDM symbols	J	4
code rate	r_{c}	$1/2$
alphabet	$\mathcal{A}$	QPSK
symbol rate	r_{s}	2
velocity	v	$\{0, 120\}$ km/h
normalized Doppler	ν_{D}	0.057
delay support	τ_{P}	1.6 μs
normalized delay	θ_{P}	0.025

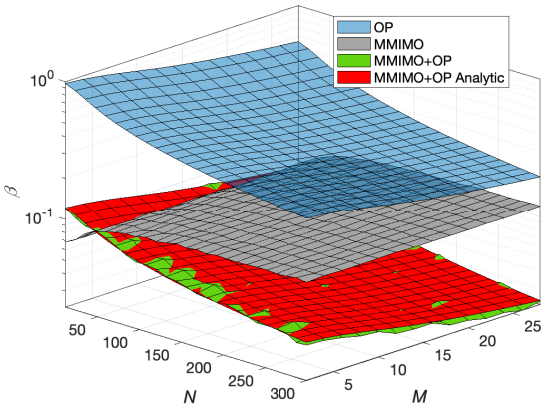

FIGURE 3. Channel hardening measure β versus M and N for OP, massive MIMO (MMIMO), as well as massive MIMO with OP (MMIMO+OP). Perfect CSI at the base station is assumed for maximum-ratio beam-forming.

VI. NUMERICAL SIMULATION RESULTS

A. SIMULATION PARAMETERS

The OFDM physical layer parameters are taken from the 5G NR standard [25], [26]. We use $N_{\text{FFT}} = 512$ subcarriers, where a maximum of 300 subcarriers can be used for data transmission, resulting in a maximum of 25 resource blocks (consisting of 12 subcarriers). For the numerical results we use 10 resource blocks for data transmission, i.e. $N = 120$ subucarriers. We choose a subcarrier bandwidth $\Delta f = 15\,\text{kHz}$. The used bandwidth is $B = N_{\text{FFT}}\Delta f = 7.68\,\text{MHz}$, the cyclic prefix length is $G = 40$ samples, the carrier frequency is $f_{\text{C}} = 5.9\,\text{GHz}$ and $A = 64$ antennas are utilized on the base station side and a single antenna at the mobile station. The demodulation reference symbols (DRS) are distributed over the OFDM frame within $J = 4$ dedicated pilot OFDM symbols at time-indices $m \in \left\{ \left\lfloor i\frac{M}{J} + \frac{M}{2J} \right\rfloor \middle| i \in \{0, \ldots, J-1\} \right\} = \{2, 6, 9, 13\}$. A quadrature phase shift keying (QPSK) symbol alphabet $\mathcal{A}$ is used with symbol rate $r_{\text{s}} = 2$ and an $r_{\text{c}} = 1/2$ convolutional code for channel coding followed by a random interleaver. We are interested in short packet lengths for URLLC packets where the convolutional code incurs only a small performance loss but provides faster decoding speed [27], [28]. The simulations parameters are summarized in Table 1.

B. GEOMETRY-BASED CHANNEL MODEL

We use a geometry-based channel model (GCM) with a flat power delay profile (PDP) and a flat Doppler spectral density (DSD) (see [7]). The mobile station moves with $v \in \{0, 120\}$ km/h.

C. CHANNEL HARDENING

In Fig. 3 the channel hardening measure $\beta(M, N; \nu_{\text{D}}, \theta_{\text{P}})$ of OP is shown for $v = 120\,\text{km/h}$, resulting in $\nu_{\text{D}} = 0.057$, and for a PDP with a support of $\tau_{\text{P}} = 1.6\,\mu\text{s}$, resulting in $\theta_{\text{P}} = 0.025$.

OP uses a time-frequency region of $2 \leq M \leq 28$ OFDM symbols and $12 \leq N \leq 300$ subcarriers. We compare three cases: (i) OP with a single transmit antenna, (ii) massive MIMO with $A = 64$ antennas (MMIMO), and (iii) massive MIMO with OP (MMIMO+OP). For massive MIMO and for massive MIMO with OP we calculate β empirically, according to (33), (44) and (46) using $F = 500$ frames. The analytic result for OP and for massive MIMO with OP are computed using (50) and (51) respectively.

Clearly the channel hardening of OP increases with growing M and N, exploiting time- and frequency diversity. Massive MIMO, on the other side, is less affected by the block size since it mainly exploits spatial diversity. The combination of massive MIMO with OP enables the utilization of spatial as well as time and frequency diversity. The channel hardening effect of massive MIMO and of OP is multiplicative for large M and N (see also (51)).

OP gains most due to frequency-diversity and less from time-diversity, since the time-bandwidth product of the fading process in frequency is larger than the one in time, i.e. $\theta_{\text{P}} N \gg \nu_{\text{D}} M$, for the used 5G NR parameters (see Table 1). The result will look different for millimeter wave carrier frequencies with $f_{\text{C}} > 30\,\text{GHz}$, since the normalized Doppler will scale linearly with f_{C}. A data transmission for URLLC should be scheduled within resource blocks taking the bound (52) into account.

In Fig. 4 we fix $M = 14$ and $N = 120$, representing a typical resource block size for URLLC traffic. We vary the normalized Doppler bandwidth $0 \leq \nu_{\text{D}} \leq 0.057$ and the normalized Delay $0 \leq \theta_{\text{P}} \leq 0.025$. As in Fig. 3, β decreases with increasing time- and frequency selectivity of the channel. Also here we can clearly observe the benefit of combining massive MIMO with OP.

Finally, we address the interesting aspect of massive MIMO with outdated CSI for beamforming, which is the central focus of this paper. In Fig. 5 we present the same plots as in Fig. 3, but now we use the last-known channel

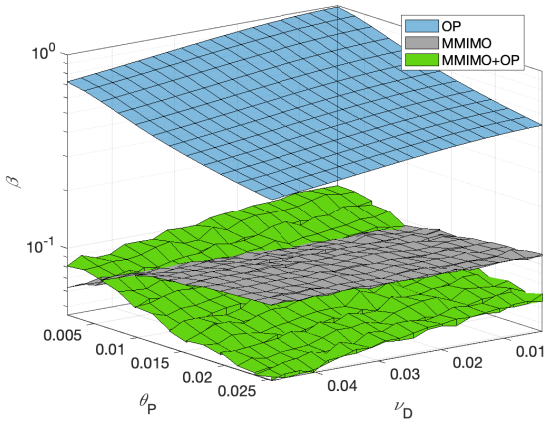

FIGURE 4. Channel hardening measure β versus ν_D and θ_P for OP, massive MIMO, and massive MIMO with OP. Perfect CSI at the base station is assumed for maximum-ratio beam-forming.

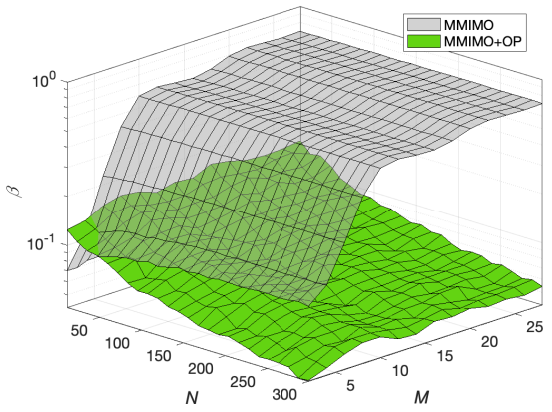

FIGURE 5. Channel hardening measure β versus M and N for massive MIMO, and massive MIMO with OP. The last-known channel state from the preceding uplink transmission (BF CSI) is used for maximum ratio beam-forming.

state from the preceding uplink transmission (BF CSI) for maximum ratio beam-forming at the base station.

The BF CSI assumption follows the frame design of the 5G NR TDD specifications [26]. Channel hardening decreases (β increases) rapidly with increasing block size in time M. By combining OP and massive MIMO a substantial channel hardening improvement can be achieved.

In Fig. 6 we fix $M = 14$ and $N = 120$ and we vary the normalized Doppler bandwidth $0 \leq \nu_D \leq 0.057$ and the normalized Delay $0 \leq \theta_P \leq 0.025$. The last-known channel state from the preceding uplink transmission is used for maximum ratio beam-forming (BF CSI).

Similarly as in Fig. 5, we see that with increasing Doppler bandwidth ν_D the channel hardening decreases for massive MIMO (β increases). For massive MIMO with OP the channel hardening is more or less constant over the range of ν_D.

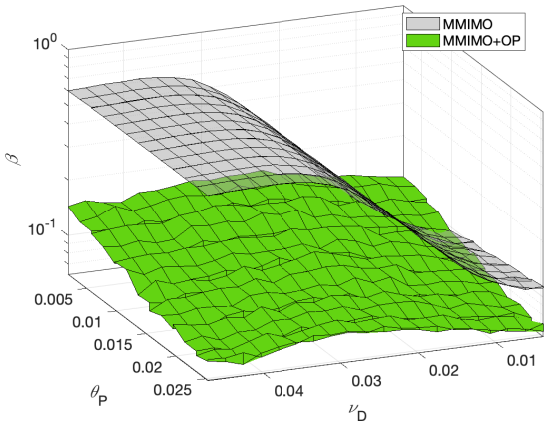

FIGURE 6. Channel hardening measure β versus ν_D and θ_P for massive MIMO, and massive MIMO with OP. The last-known channel state from the preceding uplink transmission (BF CSI) is used for maximum ratio beam-forming.

D. BIT ERROR RATE

Figs. 7-9 show numerical link level simulation results for the BER vs. bit energy E_b divided by the noise power density N_0,

$$E_b/N_0 = r_c r_s \frac{1}{\sigma_n^2} \frac{S_d}{MN} \frac{N_{FFT}}{N_{FFT} + G}, \tag{54}$$

of a wireless 5G NR link from the base station with $A = 64$ antennas to a single vehicle moving with $v \in \{40, 50, 60\}$km/h. The thin dotted reference line shows the performance of the convolutional code with additive white Gaussian noise and a single transmit antenna. Massive MIMO reaches this performance bound (not shown) in the case of perfect CSI at the base station.

All simulation results are calculated for the case of precoding at the base station using the last know CSI from the preceding uplink transmission (BF CSI) following the 5G NR TDD frame structure. We compare two transmission modes (i) massive MIMO (MMIMO) and (ii) massive MIMO with OP (MMIMO+OP). All simulations use channel estimates obtained with embedded pilot symbols on the mobile station side. Three receiver iterations are used in case of OP and two iterations are used without OP. For more iterations the performance does not improve.

In Figs. 7-9 the dashed thin line shows the performance for a single transmit antenna $A = 1$. The thin solid line displays the BER if OP with DSFT basis functions is used and $A = 1$. OP allows to utilize the time and frequency diversity reducing the BER. The BER shown for these two transmission modes is more or less constant for the simulated velocity range.

The thick dash-dotted line presents the performance of massive MIMO with $A = 64$ antennas. Maximum ratio beam-forming is employed using the last know CSI from the preceding uplink transmission (BF CSI). Due to channel aging between uplink and downlink the BER increases with increasing velocity. At $v = 50$ km/h the massive MIMO

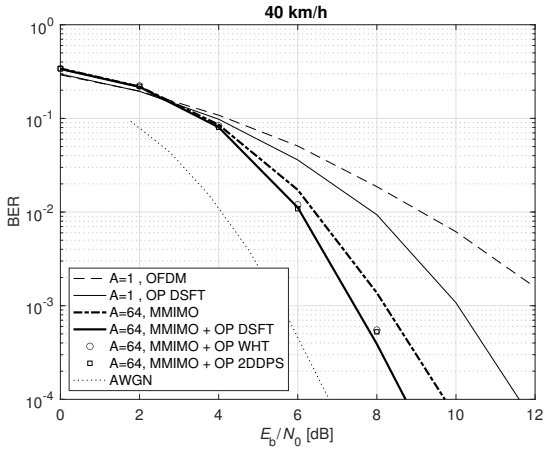

FIGURE 7. BER versus E_b/N_0 for massive MIMO with $A = 64$ antennas with and without OP using BF CSI at the base station and channel estimation at the mobile station. The thin lines show results for a single transmit antenna with and without OP. The mobile station has a velocity of $v = 40$ km/h. Furthermore, we show results for OP with Walsh-Hadamard transform sequences (WHT) as well as 2D discrete prolate spheroidal sequences (2DDPS).

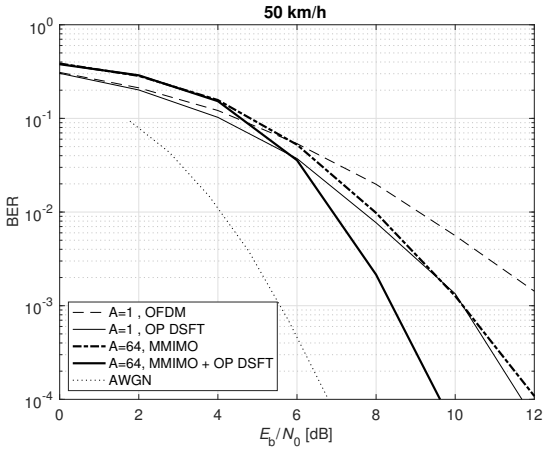

FIGURE 8. BER versus E_b/N_0 for massive MIMO with $A = 64$ antennas with and without OP using BF CSI at the base station and channel estimation at the mobile station. Furthermore we show results for a single transmit antenna with and without OP. The mobile station has a velocity of $v = 50$ km/h.

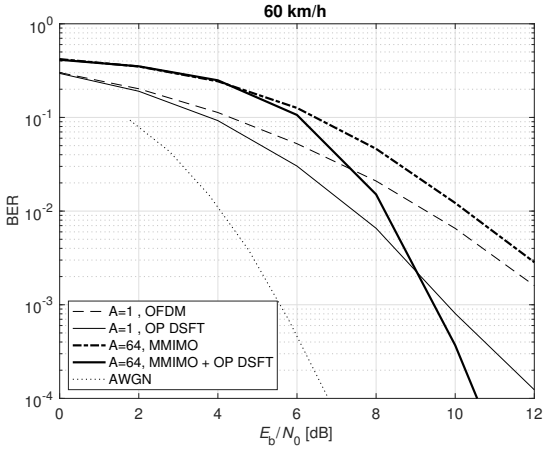

FIGURE 9. BER versus E_b/N_0 for massive MIMO with $A = 64$ antennas with and without OP using BF CSI at the base station and channel estimation at the mobile station. Furthermore we show results for a single transmit antenna with and without OP. The mobile station has a velocity of $v = 60$ km/h.

system with $A = 64$ antennas performs similar to a single antenna transmissions using OP. At $v = 60$ km/h it is even better to just use a single transmit antenna compared to massive MIMO with $A = 64$ antennas.

Finally, the thick solid lines shows the performance of massive MIMO with OP. Massive MIMO with OP is always better than massive MIMO only. Comparing massive MIMO with OP and OP for $A = 1$, we see that the crossover point in the BER figures moves to higher E_b/N_0 values with increasing velocity. For $v = 60$ km/h massive MIMO with OP can still utilize the full diversity but performs best only for an $E_b/N_0 > 9$ dB. The best strategy for velocities $v >> 60$ km/h as well as for spatial correlation is subject to our current research.

In Fig. 7 we show results for three precoding sequence sets for $v = 40$ km/h, using (i) the discrete symplectic Fourier transform (DSFT) sequences, (ii) Walsh-Hadamard transform sequences (WHT), and (iii) 2D discrete prolate spheroidal sequences (2DDPS). As explained in Sec. V-A in (37) all constant modulus sequences perform identically. The 2D DPS sequences also perform similarly.

Figs. 7-9 demonstrate that by combining massive MIMO with OP and by using an iterative receiver algorithm the BER performance can be improved by more than one order of magnitude for vehicular scenarios.

VII. CONCLUSIONS

In this paper we have investigated a new approach for vehicular ultra-reliable low-latency wireless communication (URLLC) links. For URLLC links it is highly desirable to reduce random field-strength variations causing randomly occurring errors. Appropriate processing on the transmitter and receiver side is required to obtain channel hardening by exploiting spatial, time and frequency diversity.

To achieve this goal, we combined two linear preprocessing techniques. The first one is orthogonal precoding (OP) which exploits diversity in the time-frequency domain. Its channel hardening effect increases with the delay and Doppler spread of the doubly selective fading process. The second preprocessing technique is maximum-ratio beamforming in a massive MIMO system. It achieves channel hardening that decreases with increasing velocity of the mobile station due to channel aging.

Combining massive MIMO and OP we have shown for the first time that reduced spatial channel hardening due to channel aging can be partially compensated by orthogonal precoding with two-dimensional precoding sequences in the time-frequency domain. A receiver for massive MIMO with OP using coded transmission is presented in detail.

We proved that all constant modulus sequences, e.g. discrete symplectic Fourier transform (DSFT) sequences or Walsh-Hadamard transform (WHT) sequences, lead to the same performance for OP. Furthermore, we analytically quantified the channel hardening effect of massive MIMO with OP for doubly-selective channels.

Our results are validated by link level simulation results in terms of BER vs. E_b/N_0. The combination of massive MIMO and OP improves the BER by more than one order of magnitude in time-varying vehicular scenarios using the 5G NR physical layer enabling vehicular URLLC communication links.

• • •

REFERENCES

[1] M. Shafi, A. F. Molisch, P. J. Smith, T. Haustein, P. Zhu, P. D. Silva, F. Tufvesson, A. Benjebbour, and G. Wunder, "5G: A tutorial overview of standards, trials, challenges, deployment, and practice," IEEE Journal on Selected Areas in Communications, vol. 35, no. 6, pp. 1201–1221, June 2017.

[2] T. Marzetta, "Noncooperative cellular wireless with unlimited numbers of base station antennas," IEEE Trans. Wireless Commun., vol. 9, no. 11, pp. 3590 – 3600, November 2010.

[3] S. Gunnarsson, J. Flordelis, L. Van der Perre, and F. Tufvesson, "Channel hardening in massive MIMO - A measurement based analysis," in 19th IEEE International Workshop on Signal Processing Advances in Wireless Communications (SPAWC), June 2018.

[4] H. Q. Ngo and E. G. Larsson, "No downlink pilots are needed in TDD massive MIMO," IEEE Transactions on Wireless Communications, vol. 16, no. 5, pp. 2921–2935, May 2017.

[5] K. T. Truong and R. W. Heath, "Effects of channel aging in massive MIMO systems," Journal of Communications and Networks, vol. 15, no. 4, pp. 338–351, Aug 2013.

[6] A. K. Papazafeiropoulos and T. Ratnarajah, "Deterministic equivalent performance analysis of time-varying massive MIMO systems," IEEE Transactions on Wireless Communications, vol. 14, no. 10, pp. 5795–5809, Oct 2015.

[7] T. Zemen, M. Hofer, D. Loeschenbrand, and C. Pacher, "Iterative detection for orthogonal precoding in doubly selective channels," in IEEE International Symposium on Personal, Indoor and Mobile Radio Communications (PIMRC), Bologna, Italy, September 2018.

[8] R. Hadani, S. Rakib, M. Tsatsanis, A. Monk, A. J. Goldsmith, A. F. Molisch, and R. Calderbank, "Orthogonal time frequency space modulation," in IEEE Wireless Communications and Networking Conference (WCNC), San Francisco (CA), USA, March 2017.

[9] R. Hadani, S. Rakib, A. F. Molisch, C. Ibars, A. Monk, M. Tsatsanis, J. Delfeld, A. Goldsmith, and R. Calderbank, "Orthogonal time frequency space (OTFS) modulation for millimeter-wave communications systems," in International Microwave Symposium (IMS), Philadelphia (PA), USA, June 2018, submitted.

[10] A. RezazadehReyhani, A. Farhang, M. Ji, R. Chen, and B. Farhang-Boroujeny, "Analysis of discrete-time MIMO OFDM-based orthogonal time frequency space modulation," CoRR, vol. abs/1710.07900, 2017. [Online]. Available: http://arxiv.org/abs/1710.07900

[11] T. Zemen and D. Loeschenbrand, "Combating massive MIMO channel aging by orthogonal precoding," in IEEE 5G World Forum, Dresden, Germany, September 2019, submitted.

[12] T. Zemen, C. F. Mecklenbräuker, J. Wehinger, and R. R. Müller, "Iterative joint time-variant channel estimation and multi-user detection for MC-CDMA," IEEE Trans. Wireless Commun., vol. 5, no. 6, pp. 1469–1478, June 2006.

[13] T. Zemen and A. F. Molisch, "Adaptive reduced-rank estimation of non-stationary time-variant channels using subspace selection," IEEE Trans. Veh. Technol., vol. 61, no. 9, pp. 4042–4056, November 2012.

[14] S. Verdú, Multiuser Detection. New York, USA: Cambridge University Press, 1998.

[15] T. Zemen, C. F. Mecklenbräuker, B. H. Fleury, and F. Kaltenberger, "Minimum-energy band-limited predictor with dynamic subspace selection for time-variant flat-fading channels," IEEE Trans. Signal Process., vol. 55, no. 9, pp. 4534–4548, September 2007.

[16] T. Zemen, L. Bernado, N. Czink, and A. F. Molisch, "Iterative time-variant channel estimation for 802.11p using generalized discrete prolate spheroidal sequences," IEEE Trans. Veh. Technol., vol. 61, no. 3, pp. 1222–1233, March 2012.

[17] R. R. Müller and G. Caire, "The optimal received power distribution for IC-based iterative multiuser joint decoders," in 39th Annual Allerton Conference on Communication, Control and Computing, Monticello (IL), USA, August 2001.

[18] L. R. Bahl, J. Cocke, F. Jelinek, and J. Raviv, "Optimal decoding of linear codes for minimizing symbol error rate," IEEE Trans. Inf. Theory, vol. 20, no. 2, pp. 284–287, March 1974.

[19] F. Long, K. Niu, C. Dong, and J. Lin, "Low complexity iterative LMMSE-PIC equalizer for OTFS," in ICC 2019 - 2019 IEEE International Conference on Communications (ICC), May 2019.

[20] C. Studer, A. Burg, and H. Bolcskei, "Soft-output sphere decoding: Algorithms and VLSI implementation," IEEE Journal on Selected Areas in Communications, vol. 26, no. 2, 2008.

[21] N. Fatema, G. Hua, Y. Xiang, D. Peng, and I. Natgunanathan, "Massive MIMO linear precoding: A survey," IEEE Systems Journal, pp. 1–12, 2018.

[22] M. Kollengode Ramachandran and A. Chockalingam, "MIMO-OTFS in high-Doppler fading channels: Signal detection and channel estimation in high-doppler fading channels: Signal detection and channel estimation," in IEEE Global Communications Conference (GLOBECOM), Dec 2018, pp. 206–212.

[23] W. Shen, L. Dai, J. An, P. Fan, and R. W. Heath, "Channel estimation for orthogonal time frequency space (OTFS) massive MIMO," IEEE Transactions on Signal Processing, pp. 1–1, 2019.

[24] D. Slepian, "Prolate spheroidal wave functions, Fourier analysis, and uncertainty - V: The discrete case," The Bell System Technical Journal, vol. 57, no. 5, pp. 1371–1430, May-June 1978.

[25] X. Lin, J. Li, R. Baldemair, T. Cheng, S. Parkvall, D. Larsson, H. Koorapaty, M. Frenne, S. Falahati, A. Grövlen, and K. Werner, "5G new radio: Unveiling the essentials of the next generation wireless access technology," CoRR, vol. abs/1806.06898, 2018. [Online]. Available: http://arxiv.org/abs/1806.06898

[26] TS 38.211, "NR; physical channels and modulation," V15.6.0, April 2018. Available online: https://portal.3gpp.org.

[27] B. Tahir, S. Schwarz, and M. Rupp, "BER comparison between convolutional, turbo, LDPC, and polar codes," in 24th international conference on telecommunications (ICT). IEEE, 2017, pp. 1–7.

[28] O. Iscan, D. Lentner, and W. Xu, "A comparison of channel coding schemes for 5G short message transmission," in 2016 IEEE Globecom Workshops. IEEE, 2016, pp. 1–6.

THOMAS ZEMEN (S'03–M'05–SM'10) received the Dipl.-Ing. degree (with distinction) in electrical engineering in 1998, the doctoral degree (with distinction) in 2004 and the Venia Docendi (Habilitation) for "Mobile Communications" in 2013, all from Vienna University of Technology. From 1998 to 2003 he worked as Hardware Engineer and Project Manager for the Radio Communication Devices Department, Siemens Austria. From 2003 to 2015 Thomas Zemen was with FTW Forschungszentrum Telekommunikation Wien and Head of the "Signal and Information Processing" department since 2008. Since 2014 Thomas Zemen is Senior Scientist at AIT Austrian Institute of Technology. He is the author or coauthor of four books chapters, 35 journal papers and more than 105 conference communications. His research interests focus on wireless ultra-reliable low-latency communication (URLLC) systems for autonomous vehicles and industrial production environments; 5G massive MIMO systems; time-variant channel measurements, modeling and real time emulation; software-defined radio rapid prototyping, and indoor localization. Dr. Zemen is docent at Vienna University of Technology and serves as Editor for the IEEE Transactions on Wireless Communications.

DAVID LOESCHENBRAND received the Dipl.-Ing. degree (with distinction) in Telecommunications in 2016 from Vienna University of Technology. From 2012 to 2015, he worked for the Institute of Telecommunications, implementing software for antenna characterization purposes. Since 2016, he is a Ph.D. candidate with the Austrian Institute of Technology in the group of Thomas Zemen. His research interests focus on massive MIMO in time-varying propagation channels, channel aging, antenna design, reliable low-latency wireless communications for highly autonomous vehicles, vehicular channel measurements and channel modelling. He gained experience in research work and project management during several finished and ongoing applied research projects on a national and international scale. He successfully implemented a software defined radio based massive MIMO testbed for highspeed measurements and signal processing experimentation, which provides crucial insights for several of AIT's projects.

MARKUS HOFER received the Dipl.-Ing. degree (with distinction) in telecommunications from the Vienna University of Technology, Vienna, Austria, in 2013. Since 2013, he has been working toward the Ph.D. degree in telecommunications. From 2013 to 2015 he was with the FTW Telecommunications Research Center Vienna working as a Researcher in "Signal and Information Processing" department. Since 2015, he has been with the AIT Austrian Institute of Technology, Vienna, as a Junior Scientist in the research group for ultrareliable wireless machine-to-machine communications. His research interests include low- latency wireless communications, time-variant channel measurements, modeling and realtime emulation; time-variant channel estimation, 5G massive MIMO systems; software-defined radio rapid prototyping, cooperative communication systems, and interference management.

CHRISTOPH PACHER received the Dipl.-Ing. degree (with distinction) in electrical engineering from the University of Technology in Vienna in 1999. From 1999 to 2003 he was research assistant at TU Vienna and worked on both experimental and theoretical quantum transport in semiconductors. In 2004, he joined AIT Austrian Institute of Technology and developed algorithms and software for optoelectronic simulations. In 2007 he received the doctoral degree in technical sciences (with distinction) from TU Vienna and started in the EU-FP6 project SECOQC his work on the theory of and on algorithms for post processing for QKD and QRNG at AIT. He was a visiting researcher at ETH Zurich in the group of Prof. R. Renner (2011) and the University of South Australia (2013). He participated as scientist, WP leader, steering-committee member and project manager in several national and international research projects in the context of quantum cryptography and is co-author of more than 30 journal papers and 20 conference proceedings. In 2018, Christoph Pacher has been appointed Senior Scientist and group leader of the Optical Quantum Technology group at AIT. His current research interests focus around algorithms for and theory of quantum cryptographic primitives (quantum key distribution, quantum random number generation, and quantum oblivious transfer), and information theoretic security.

BENJAMIN RAINER is a researcher in AIT's Center for Digital Safety & Security. He received the M.Sc. (Dipl.-Ing.), and Ph.D. (Dr. techn.) in computer science all with distinction from the Alpen-Adria-University Klagenfurt. His research interests are security and communication in future (mobile) networks with emphasises on routing, forwarding caching and wireless channel modelling. He is currently working in AIT's Wireless research group led by Thomas Zemen.